Chapter 3. Materials Characterization Techniques

This chapter explains the fundamental and operations of different characterization techniques that have been utilized in order to characterize the physical and chemical features of the synthesized and developed materials in this thesis.

3.1 Electron microscopy

Electron microscopy provides an excellent opportunity for studying the microstructure of materials with much higher magnification and resolution than optical microscopy. While the detection of features smaller than about 1 μm is not possible by optical microscopy, electron microscopy reveals details with a resolution of ~ 0.1 nm. This is simply because the wavelengths of electron beams are about 10000 times shorter than that of visible light (a few hundred nanometers). In an electron microscope, the interaction between the focused beam of high-energy electrons (100-400 keV) and the sample leads to many detectable signals including: transmitted electrons, diffracted electrons, secondary electrons, back-scattered electrons, auger electrons, and X-rays (). Therefore, the electron microscopy can provide a wealth of information on morphology, crystallography, and chemical composition of materials. The most commonly used electron microscopy techniques are transmission electron microscopy (TEM) and scanning electron microscopy (SEM).

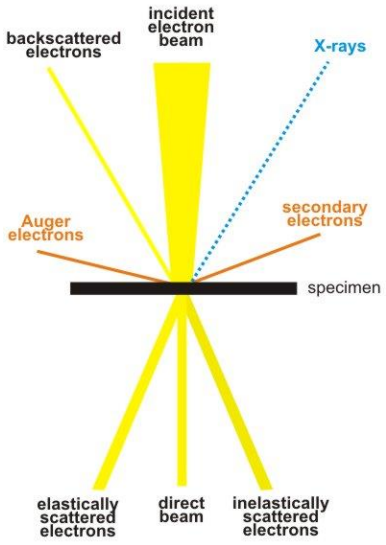

Figure 3.1. Interaction between the electron beam and the sample.

3.1.1 Transmission electron microscopy

The schematic diagram of a typical transmission electron microscope is shown in Figure 3.2. This instrument, which is in a sense similar to an optical microscope, consists of three main parts: electron gun, electromagnetic lenses, and specimen stage. The electron gun generates a primary

electron beam of high energy and high intensity, which hits the sample after passing through condenser lenses. It is worth reminding that the condenser lenses control the diameter and the convergence angle of the beams. The intensity of the electron beam decreases as it is transmitted through the specimen. The decrease in the intensity of a beam, or attenuation, strongly depends on the density and the thickness of sample. Therefore, the transmitted electrons create a two-dimensional projection of the sample mass, which is afterward magnified by the electromagnetic lenses to produce a so-called bright-field image. At the same time, the diffracted electron beams that are marginally off-angle from the transmitted electron beam form a so-called dark-field image.

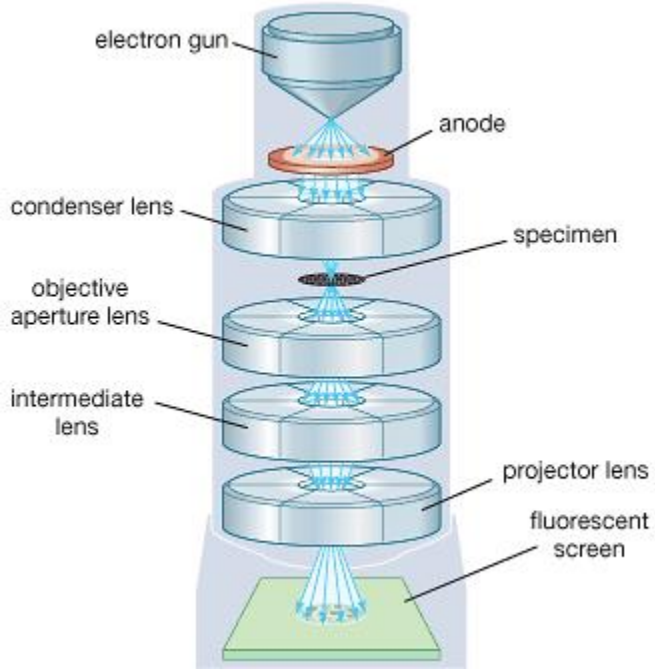

Figure 3.2. Structure of a transmission electron microscope and the optical path.

TEM, with a high resolution of 0.3 nm, is the most commonly applied form of electron microscopy for studying supported catalysts. Usually if the contrast between the particles and support are sufficient, their detections are possible. This may impede applications of TEM on well-dispersed supported oxides. Contrast in the transmission mode is caused not only by the attenuation of electrons due to intensity and thickness variations over the sample, but also by diffraction and interference.

3.1.2 Scanning electron microscopy

The scanning electron microscope (SEM) is an electron microscope that examines microscopic structure of the sample via scanning its surface with high resolution and great depth. An image is generated by a focused electron beam that scans over the surface area of the sample. It should be mentioned that the most important feature of SEM images is the three-dimensional appearance of the sample. Moreover, SEM system could provide chemical information of a sample via X-ray energy dispersive spectrometer (EDS). Similar to TEM system, SEM possesses an electron gun and a series of electromagnetic lenses and apertures. Nevertheless, the electron beam is condensed to a fine probe for surface scanning. Its brightness has more important role in imaging quality in SEM rather than TEM. The acceleration voltage for generating an electron beam is in the range 1–40 kV, which is about one order of magnitude less than that for a TEM.

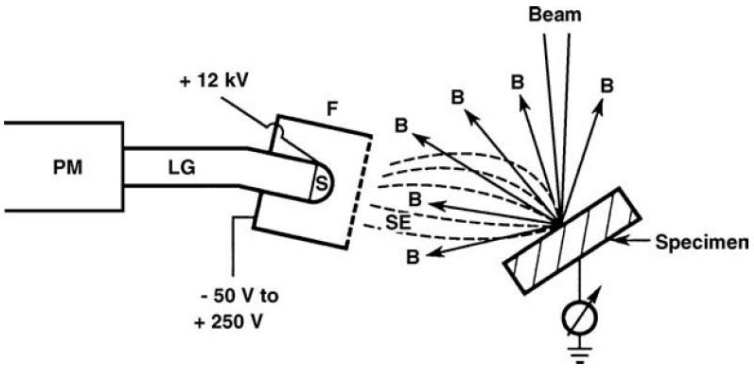

Figure 3.3. Signal collection by the Everhart–Thornley detector. B, backscattered electron trajectory; SE, secondary electron trajectory; F, Faraday cage; S, scintillator; LG, light guide; PM, photomultiplier tube.[302]

SEM functionality depends on two kinds of scattering: elastic and inelastic. Incident electrons scatter by atoms in the sample are elastic scattering or the backscattered electrons. They are usually deflected at large angles and with little energy losses (20-40% energy loss). Electrons ejected from atoms in the material create secondary electrons which is called inelastic scattering. These ones are normally deflected at small angles and possess significantly lower energy in comparison with incident electrons. During inelastic scattering, an incident electron transfers kinetic energy to an electron in a specimen atom. Any electron in atoms in the specimen with sufficient kinetic energy will leave its orbital to become a secondary electron (Figure 3.3).

Secondary electrons are responsible for obtaining topographic contrast, while backscattered electrons are used to gain information of elemental composition contrast.

3.2 Nitrogen physisorption

Surface area and pore size distribution of porous materials can be determined through physisorption isotherm analysis. The physisorption isotherm is defined as a plot of the amount of adsorbed gas against the equilibrium relative pressure (P/P_0) at a constant temperature.

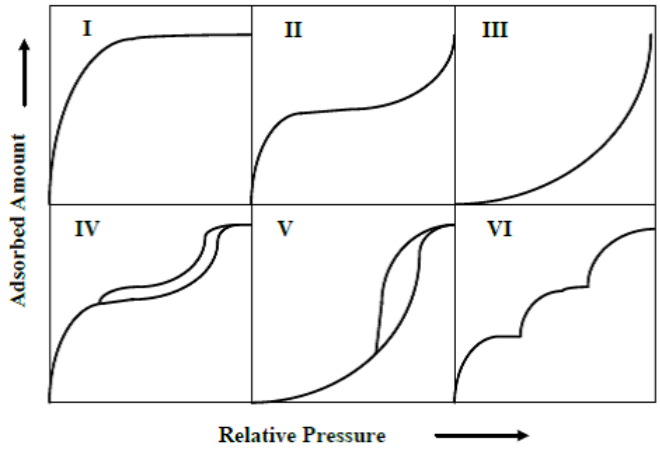

Figure 3.4. Different kinds of physisorption isotherms.

As it can be seen in Figure 3.4, there are different kinds of physisorption isotherm. Microporous materials show the Type I isotherm that is reversible. In this kind of isotherm, there is a rapid rise at low pressures related to monolayer adsorption and a plateau at higher pressures because of micropores filling. Non-porous or macroporous materials represent the reversible Type II and III isotherms. In the Type II isotherm, monolayer adsorption completes at point B and multilayer adsorption begins. In the Type III isotherm, which is an uncommon form of isotherm for non-porous or macroporous materials, the role of adsorbate-adsorbate interactions is significant. Mesoporous materials exhibit the Type IV and V isotherms with the main characteristic of hysteresis loop due to capillary condensation. In the uncommon Type V isotherm, which is related to Type III isotherm, the adsorbent-adsorbate interaction is weak. Uniform non-porous materials display the Type VI isotherm, which is typical of stepwise multilayer adsorption.[303]

Hysteresis loop, the main feature of the Type IV isotherm, is related to capillary condensation in mesoporous materials and happens when the adsorption and desorption graphs do not coincide. Different types of hysteresis loops are illustrated in Figure 3.5. Type H1 hysteresis, which in that there are almost vertical and nearly parallel adsorption/desorption curves over a wide range of P/P_0, is given by cylindrical pores with a narrow pore size distribution. Type H2 hysteresis, including of a desorption curve far sharper than the adsorption curve, is displayed by 'ink-bottle' pores with narrow necks and wide bodies. Type H3 and H4 hysteresis loops are related to slit-shaped pores and narrow slit-like pores, respectively.[304]

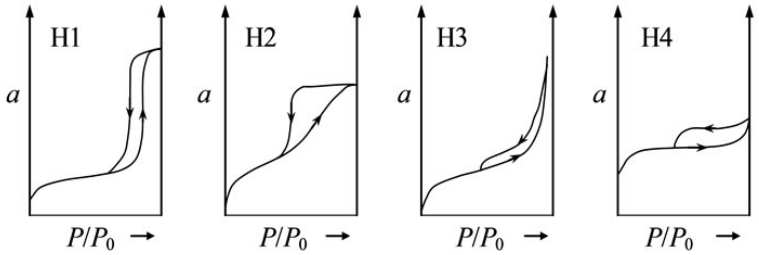

Figure 3.5. Different kinds of hysteresis loops.

To date, various theories are introduced to specify the surface area of porous materials among them the Brunauer-Emmett-Teller (BET) theory is the most widespread method. The BET equation is usually given in the following form

$$\frac{P/P_0}{n(1-P/P_0)} = \frac{1}{n_m c} + \frac{c-1}{n_m c} \times \frac{P}{P_0} \qquad (3.1)$$

A linear relationship between $\frac{P/P_0}{n\,(1-P/P_0)}$ and P/P_0 is obtained by the BET equation. The intercept $\frac{1}{n_m c}$ and slope $\frac{c-1}{n_m c}$ can be used to calculate the values of n_m and c. Therefore, the surface area can be computed from the monolayer capacity on the assumption of close packing:

$$A = n_m \alpha_m L \qquad (3.2)$$

where α_m is the molecular cross-sectional area; n_m is the monolayer capacity and L is the Avogadro constant. It is indeed supposed that nitrogen is the most appropriate gas for surface area

determination. If it is assumed that the BET monolayer is close-packed, α_m will be 0.162 nm^2 at 77 K.

3.3 Photoluminescence spectroscopy

Luminescence is a photon emission process that differs from refraction, reflection and scattering of light in which it happens through electron excitation stages. They include excitonic transition, intrinsic electron transitions between energy bands, and extrinsic electronic transitions at impurities and defects of semiconductors, insulators, and organic molecular solids. Photoexcitation via optical photon absorption is called photoluminescence (PL). PL is spontaneous emission of photons, whereas stimulated photon emission plays an important role in solid-state and semiconductor lasers. This method is zero-background test and so it is a sensitive optical technique for analysing the structure of different materials including organic and inorganic materials, semiconductors and insulators. In this characterization, an energy from absorbing a photon can excite an electron from its ground state within femtosecond timescale. If there are multiple excited states as in organic molecules, then electrons excited to higher excited states rapidly relax to the lowest excited states by exciting molecular vibrations in molecules or emitting phonons in solids in picosecond order. After that, the excited electrons recombine radiatively to the ground state by emitting photons. As a result, the emitted photons are usually lower in energy than the adsorbed photons.

PL consists of two individual one-photon steps, that is, photon absorption is succeeded by photon emission with a transition time of more than 0.1 ns. The HOMO (highest occupied molecular orbital) state and the LUMO (lowest unoccupied molecular orbital) state correspond to the valence band (VB) edge and the conduction band (CB) edge, respectively. PL of semiconductors and ionic crystals is classified into two categories, intrinsic PL and extrinsic PL. Intrinsic PL happens with the band-to-band radiative transition in a highly pure semiconductor at a relatively high temperature, where an electron and a hole are excited in CB and VB, respectively, via photon adsorption. Then, they radiatively recombine to give rise to intrinsic PL. It should be noted that donors and acceptors are intentionally generated in the semiconductor via impurities. The other PL occurs between an electron trapped by a neutral donor state D^0 and a hole at the top

of VB and between an electron at the bottom of CB and a hole of the neutral acceptor state A^0. Bound excitons are generated by the capture of a free exciton by a neutral impurity state (neutral donor D^0 or acceptor A^0), ionized impurity state (ionized donor D^+ or acceptor A^-), or by a defect. Bound excitons recombination dominates over free exciton recombination for a less pure material and shows a sharp line in the highly-resolved PL spectrum at a low temperature. Excitonic recombination procedures become more important in semiconductor quantum wells, quantum wires, and QDs, where the excitonic PL can be observed even at much higher temperatures due to the increased exciton binding energy by quantum confinement. When both types of impurities are present as compensated semiconductors, donor to acceptor pair (DAP) recombination occurs through radiative tunneling. Figure 3.6 demonstrates various radiative recombination processes with impurities.

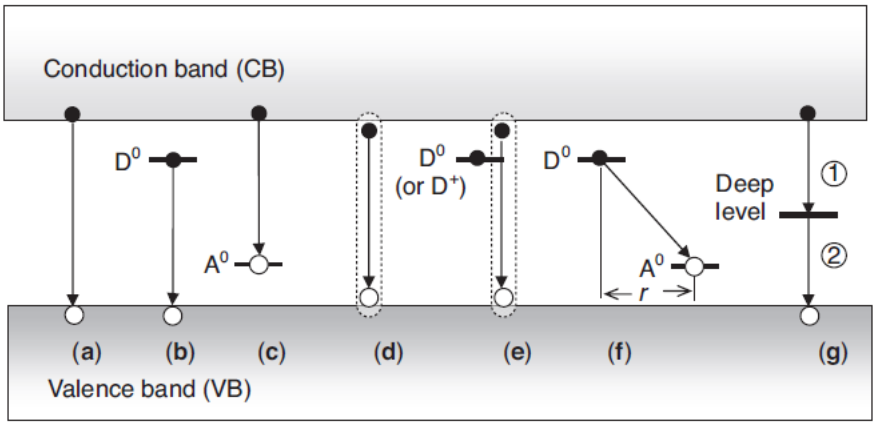

Figure 3.6. Schema of radiative recombination processes in semiconductors. (a) Band-to-band recombination, (b) neutral donor (D^0) to VB transition, (c) CB to neutral acceptor (A^0) transition, (d) radiative recombination of FE, (e) radiative recombination of BE, which is bound to D^0 (recombination of BE bound to ionized donor D^+ is also possible), (f) DAP recombination with separation r, and (g) deep-level defect luminescence (either one of the two transitions (1) and (2) is radiative).[305]

A schematic of steady-state PL spectroscopy instrument is shown in Figure 3.7. Its light excitation source can be any laser with emission energy larger or close to the sample bandgap. Using band-pass filter (BPF) is essential to eliminate the plasma line of the gaseous laser or unwanted laser lines like harmonic generation. After producing emission and illuminating on the sample, the emission from it is collected with monochromator to acquire the PL spectrum, which

is PL intensity versus wavelength or photon energy. PL can be detected via different detectors such as a photomultiplier tube, which is the most sensitive detector with high-speed response.

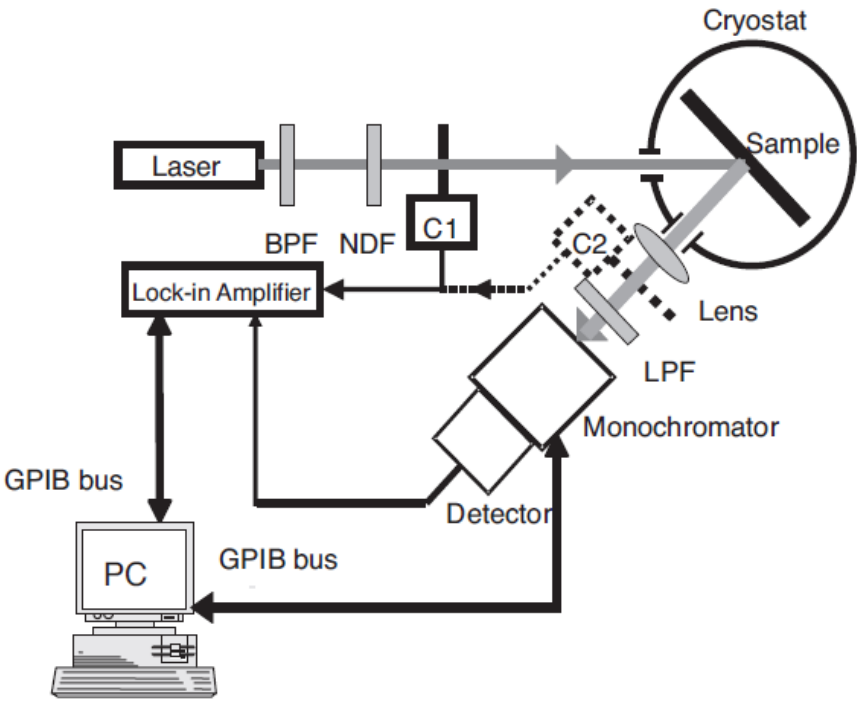

Figure 3.7. Experimental setup of static PL spectroscopy. C1,optical chopper at normal position; C2, optical chopper for long-lived PL decay measurement; BPF, band-pass filter; NDF, neutral density filter; LPF, long-pass filter; PC, personal computer.

3.4 UV-visible spectroscopy

Ultraviolet–visible spectroscopy or ultraviolet-visible spectrophotometry (UV-Vis or UV/Vis) analyazes the wavelength dependent interaction of photons with a material. It measures the attenuation of a beam light after it passes through a sample or after reflection from a sample surface. Absorption measurements can be at a single wavelength or over an extended spectral range. The UV-vis absorbance can be classified into two group: transmission and diffuse reflectance spectroscopies.

Transmission UV-vis spectroscopy is usually utilized with a sample transparent enough to allow photons pass through it. As it can be seen in Figure 3.8, the UV-vis light is pass through a solution (or thin film), and the transmitted light is collected by a detector. The difference between a transmitted light from a reference and a target sample is displayed in the figure. This technique

is generally used to analyze the organic dyes, metal or semiconductor nanoparticles highly dispersed in a solution. In an ideal solution, there is a linear relation between the absorbance wavelength and concentration. A calibration curve is prepared by plotting the absorbance of a series of standard samples as a function of their concentration and so the concentration of an unknown sample can be determined via measuring its absorbance.

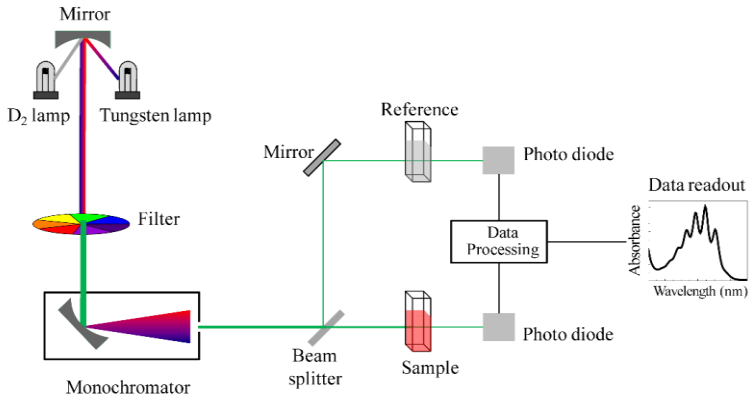

Figure 3.8. Schematic of transmission UV- visible spectrophotometer.

When the sample is not transparent and so it absorbs 100% across the entire wavelength, diffuse reflectance UV-vis spectroscopy is utilized. In general, the light beam is irradiated on the sample resulting to have light reflection in all directions. This reflected light is collected by an integrating sphere and then analyzed with a detector (Figure 3.9). This method is used to characterize the optical properties of semiconductors and metal samples in the powder form.

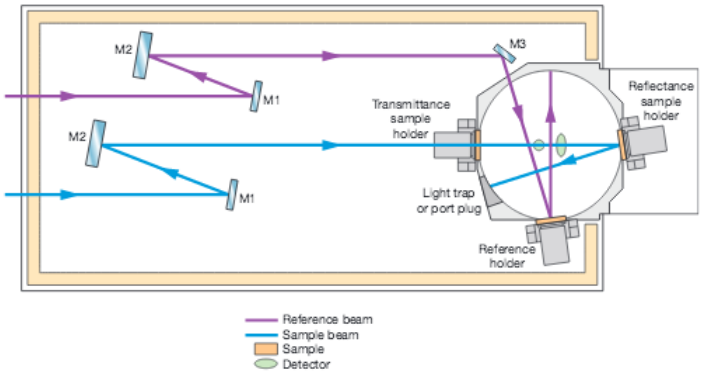

Figure 3.9. Schematic of Diffuse reflectance UV- visible spectrophotometer

3.5 Fourier Transform Infrared Spectroscopy

Generally, vibrational spectroscopy is a method to determine the molecules structures by measuring the interaction between electromagnetic radiation and nuclear vibrations in molecules. This technique employs electromagnetic waves with longer wavelength (in order of 10^{-7}), which are typically related to infrared light. Vibrational spectroscopy detects the molecular vibrations by the absorption of infrared light or by the inelastic scattering of light by a molecule. This technique can be utilized to examine the molecules structures of inorganic and organic materials in gas, liquid or solid phases. Nonetheless, it cannot analyze metallic materials due to their strong electromagnetic reflections. When a molecule is irradiated by infrared electromagnetic waves, one frequency may match the vibrational frequency of the molecule. Therefore, the molecular vibration will be excited by waves with the frequency. The excitation means that the energy of molecular vibration will increase. In the meantime, the electromagnetic radiations with the specific frequency will be absorbed by the molecule because the photon energy is transferred to excite molecular vibrations.

Fourier transform infrared spectroscopy (FTIR) is the most widely used vibrational spectroscopic technique that the Fourier transform method is utilized to obtain an infrared spectrum in a whole range of wavenumbers simultaneously. It differs from the dispersive method, which entails creating a spectrum by collecting signals at each wavenumber separately. The most important part of FTIR is the Michelson interferometer (Figure 3.10). It consists of two mirrors and a beam-splitter. The beam-splitter transmits half of the infrared beam from the source and reflects the other half. These two beams hit two mirrors and then they combine again to illuminate on the sample before reaching to a detector. The moving mirror act as a changer for the optical path lengths to create light interference between two split beams. If its distance is the same as the fixed mirror, the optical paths for both are the same. The difference in optical paths has the same affect of diffraction in crystallographic planes. The two split beams exhibit constructive and destructive interference periodically. A figure of light interference intensity as function of optical path difference is interferogram, as can be seen in Figure 3.11. The sharp center burst related to the position of the moving mirror considering as zero path difference with the maximum intensity of the interferogram. Then, by applying Fourier transform formula, the interferogram converts to the infrared spectrum, as demonstrated in Figure 3.11.

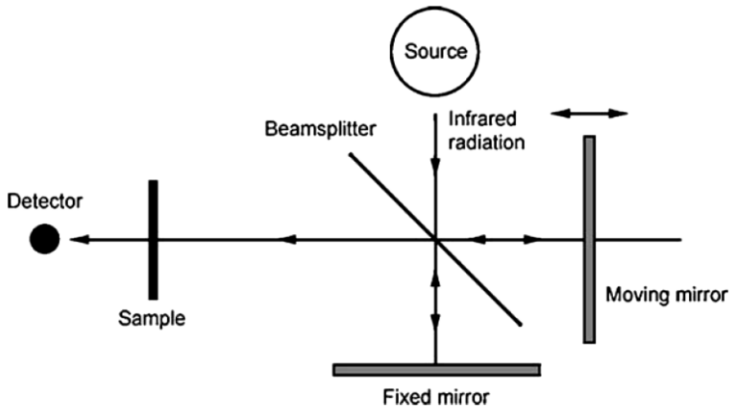

Figure 3.10. Optical diagram of a Michelson interferometer in FTIR.

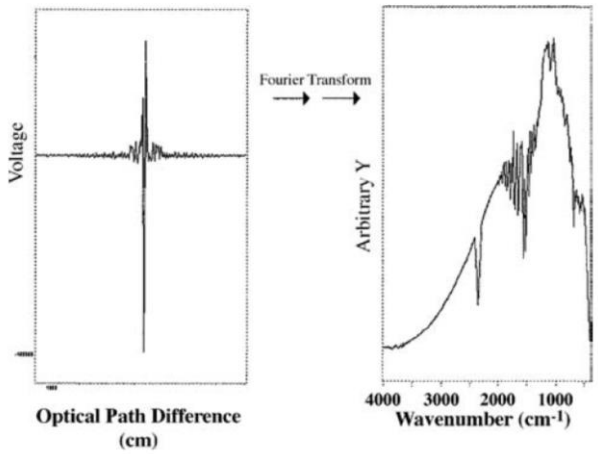

Figure 3.11. Plots of: (left) an interferogram; and (right) a Fourier transform from an interferogram to an IR spectrum.[306]

3.6 Atomic Force Microscopy

Atomic force microscope (AFM) is a technique to map sample topography. It detects near-field forces between its very sharp tip and the sample surface. There are several kinds of near-field forces including short-range, Van der Walls, electrostatic and capillary forces. The short-range forces refer to atomic forces between atoms when their distance is close to atomic spacing. The van der Waals forces are the interactive forces between dipoles of molecules. Electrostatic forces are the interactive forces between the electric charges of tip and sample. Finally, capillary forces are forces resulting from water vapor condensation between tip and sample. The key element in this characterization is the microscopic force sensor and the most widely used one is a cantilever.

The tip is loaded at the end of a cantilever and the force detection is based on a beam reflection technique as shown in Figure 3.12. The cantilever bends elastically when there is a force between the tip and sample. The amount of bending is monitored and recorded by position-sensitive photodiodes which are arranged in four quadrants. Any small deflection of the cantilever will tilt the laser beam and change its striking position on the photodiodes. The difference between the two photodiode signals indicates the amount of cantilever deflection. The amount of deflection, in turn, can be mathematically converted into the force on the tip, according to the elastic properties of the cantilever.

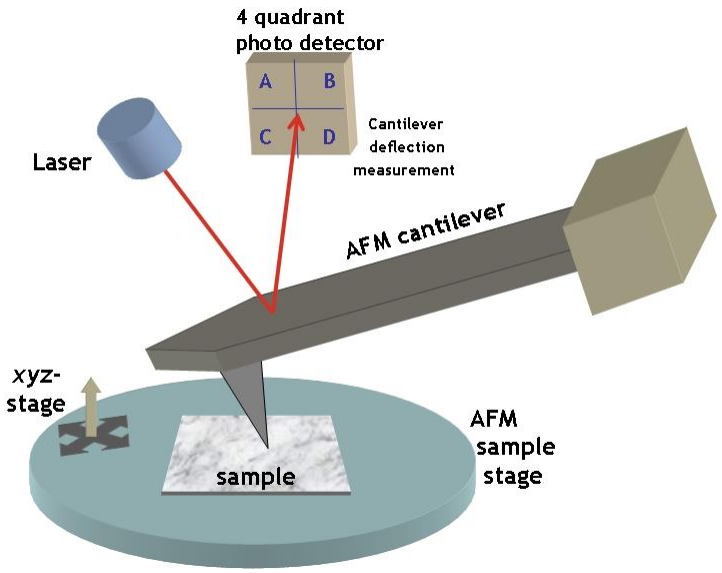

Figure 3.12. Atomic force microscope block diagram.

3.7 X-ray Diffractometry

X-ray diffractometry (XRD), one of the most widely used techniques in materials characterization, is applied to identify crystalline phases and to obtain an indication of crystallite size. X-ray diffraction is the elastic scattering of X-ray photons by atoms in a periodic network. The scattered monochromatic X-rays that are in phase produce constructive interference, which leads to a new wave that has a higher amplitude (diffraction peak). It is worth reminding that the waves are said to be in phase when their crests and troughs occur simultaneously. Figure 1.1 shows how the wavelength of the X-rays (λ), the distance between two network planes (d), the angle

between the incoming X-rays and the reflecting lattice plane (θ), and the order of interference (n) are related by the Bragg equation[307]:

$$n\lambda = 2d \sin\theta \qquad (3.3)$$

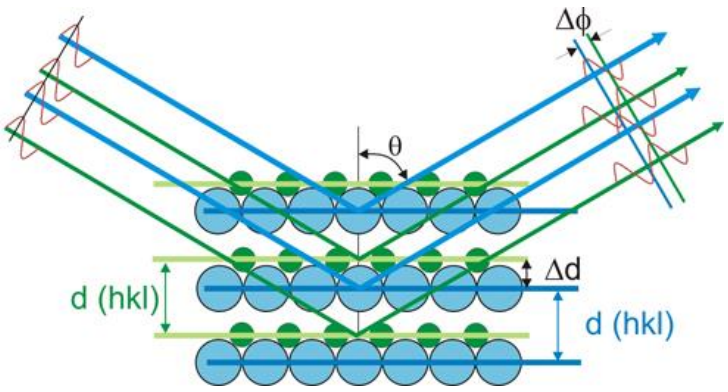

Figure 3.13. Schematic illustration of the Bragg's law.

A typical XRD instrument consists of three main parts: X-ray tube, specimen stage, and X-ray detector. The X-ray beam generated by the X-ray tube passes through special slits, which collimate the X-ray beam and prevent beam divergence. After passing through the slits, the X-ray beam strikes the specimen that is supported by the plane of specimen. The X-rays diffracted by the specimen interfere constructively when they are in phase and produce a convergent beam at receiving slits before entering the detector. By continuously changing the incident angle of the X-ray beam, diffraction intensity is recorded in a range of 2θ. The obtained spectrum is compared with a database consisting of over 60,000 diffraction spectra of known crystalline materials to identify the crystalline phases.

The XRD technique has one important limitation; the sample must possess sufficient long-range order in order to observe clear diffraction peaks. This limitation, however, has an advantage, which is that the width of diffraction peaks provides information on the dimensions of the reflecting planes. While diffraction lines from perfect crystals are very narrow, line broadening occurs for crystallite sizes below 100 nm because of incomplete destructive interference in scattering directions. The Scherrer equation relates crystallite size to line width:

$$\langle L \rangle = \frac{K\lambda}{\beta \cos\theta} \qquad (3.3)$$

where <L> is the dimension of the particle; λ is the X-ray wavelength; β is the peak width; θ is the angle between the incoming X-rays and the reflecting lattice plane; K is a constant.

3.8 X-ray photoemission spectroscopy

X-ray photoemission spectroscopy (XPS) is a technique that utilizes characteristic electron emitted from a solid for analyzing surface chemicals. The features of emitted electron not only quantitively identify the chemical composition of the target sample, but also the chemical states of its elements can be detected.

It works based on the fact that if an atom absorbs an X-ray photon with energy of hν, an electron with binding energy of E_b is ejected out of atom with a kinetic energy of:

$$E_k = h\nu - E_b - \varphi \qquad (3.4)$$

where E_k is the kinetic energy of the photoelectron; h is Planck's constant, ν is the frequency of the exciting radiation; E_b is the binding energy of the photoelectron with respect to the Fermi level of the sample and φ is the work function of the spectrometer.

In XPS analysis, the intensity of photoelectrons as a function of their kinetic energy is measured and with this equation, the kinetic energy can be converted to binding energy (usually placed on x-axis of spectrum). Binding energy of an electron exhibits the characteristic of the element from which the photoelectron originates. In addition, it can be used to identify the chemical state of the element because the energy levels of core an electron rely slightly on the chemical state of the atom. Therefore, small shifts in binding energy (less than 3 eV) shows various chemical states in atom. Generally, the binding energy of an atom, increases with increasing oxidation state and with the electronegativity of the ligands for a fixed oxidation state.

3.9 Photocatalytic test

The main goal of this thesis is to synthesize or develop a photocatalyst for generating hydrogen under visible light. The performance of original (for comparison) and developed photocatalysts are measured with photocatalytic testing system, as shown in Figure 3.14. The reactor is made of stainless steel with a Pyrex glass window on its top. Above it, there is a solar

simulator with capability of loading various light filters. Moreover, a magnetic stirrer is used to have a good mixing in the liquid phase, which is normally consists of water and a sacrificial agent with a concentration of 10-15% (volume%). An external gas pump helps to have homogenous concentration of hydrogen throughout the system. After deposition of cocatalysts via photodeposition technique, the reactor is purged with nitrogen for 10 min and then the mixture is illuminated with light beam from solar simulator with full spectrum or other light filters. After several hours, a small sample of gas phase is taken and injected to GC for analyzing its H_2 concentrations.

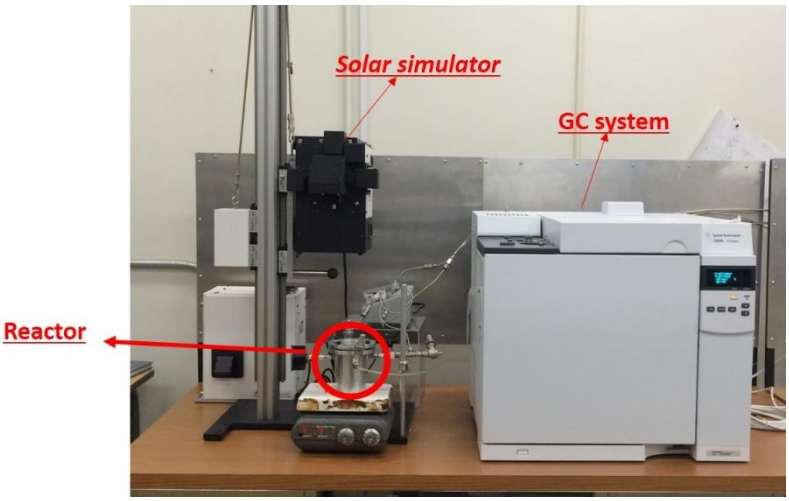

Figure 3.14. A picture of photocatalytic test for hydrogen production under solar simulator.

3.10 Synthesis methods of developed materials

3.10.1 Titanate nanodisks

To synthesize titanate nanodisks with diameter of around 20 nm, 2g of titanium butoxide, 12g of oleylamine, 12g of benzyl alcohol (oleylamine:benzyl alcohol weight ratio of 1:1) and 30g of benzyl ether were added to a 100-mL round-bottom flask.[308] The reaction mixture was heated to 190 ºC at the heating rate of 5 ºC/min under nitrogen flow. After 20 h, the reaction was stopped and cooled down to room temperature. After addition of excess absolute ethanol, the titanate nanodisks were obtained by centrifugation and redispersed in toluene and re-precipitated by ethanol for three times in order to remove the unreacted reagents.

Then, 5 mmol of as-synthesized titanate nanodisks (according to Ti atom) were dispersed in a mixture of tetraethyl ammonium hydroxide (15 mmol), ethanol (15 ml) and water (15 ml). The mixture was stirred overnight at room temperature. To the clear solution obtained was added access acetone to precipitate titanate nanodisks. The precipitate was then washed several times with acetone and finally dispersed in 10 ml of water.

3.10.2 Bulk graphitic carbon nitride

Bulk material of graphitic carbon nitride (g-C_3N_4) was synthesized from two different precursors.[309, 310] In the chapter 4, the bulk material was produced from melamine. Typically, 10 g melamine was heated in a crucible to 550 ºC and kept at this temperature for 3 h. Then, the obtained yellow powder was grounded and washed with water and ethanol several times. After that it was dried completely in an oven at 70 ºC overnight. In chapter 5, the bulk material of g-C_3N_4 was created from dicyandiamide. The precursor was calcined in a muffle furnace at 550 ºC in air for 4 h. Then, the obtained material was washed with distilled water to remove unreacted chemicals and then it was dried in an oven overnight at 70 ºC.

3.10.3 Carbon nitride nanosheets by liquid exfoliation

After synthesizing bulk g-C_3N_4, nanosheets of carbon nitride via liquid exfoliation method was synthesized as follows [154, 169]: 1 g of bulk g-C_3N_4 was added to a mixture of 100 ml isopropanol and 100 ml water, Then, the mixture was put in ultrasonication bath for 12 h. After this step, dispersed nanosheets of g-C_3N_4 were separated from residual bulk material (aggregates) with centrifugation at 3,000 rpm for 10 min. Then, the obtained nanosheets were centrifuged at 10,000 rpm for 15 min and dried at 70 ºC.

3.10.4 Carbon nitride nanosheets by gas template method

In this method, nanosheets of g-C_3N_4 were synthesized by one step calcination method.[167] First, 15 g of ammonium chloride was dissolved in 300 ml of water and then 3 g melamine was added to the mixture. Later, it was heated to 60 ºC in order to remove water and then, it was dried completely overnight. After this step is completed, the white powder was heated to 550 ºC in a semi-closed system and was kept for 4 h. After cooling down, the nanosheets were washed several times with ethanol and water and dried in oven.

3.10.5 Post-calcined graphitic carbon nitride

In chapter 5, after synthesizing bulk g-C_3N_4, it was heated again up to 650 ºC under argon gas flow of 200 mL/min for 2 h. Then, the obtained material was re-calcined in air in a muffle furnace at 500 ºC for 2 h. Later, the developed material was washed several times with water to remove contaminants and dried in an oven at 70 ºC.

3.10.6 Zinc cadmium sulfide solid solution

Zinc Cadmium sulfide solid solutions were synthesized as follow: First, 50 mL of glycerol was dissolved in 200 mL isopropanol. Typically, 1.5 mmol of zinc nitrate and 1.5 mmol of cadmium nitrate were dissolved in the mixture in order to have Zn/Cd ratio of 50%/50% (for all other samples the total mole of 3 mmol was considered constant and only the ratios of Zn/Cd were changed). Then, the mixture was transferred to an autoclave and was heated to 180 ºC for 6h. Later, the synthesized material was collected via centrifugation at 5,000 rpm and dried at 70ºC overnight. The obtained sample was calcined in air at 500ºC for 4 h to acquire zinc and cadmium mixed oxide. Subsequently, the mixed oxide was exposed to a flowing gas mixture of H_2S (10%)/Ar at 450ºC for 2 h. Therefore, sulfide (S^{-2}) ions could substitute with oxygen and so the mixed oxide was converted to a mixed sulfide.